PCCP

Physical Chemistry Chemical Physics

This paper was published in a themed issue of *PCCP* on:

Colloidal particles at liquid interfaces

Guest Editor: Professor B. P. Binks

Please take a look at the full table of contents for this issue

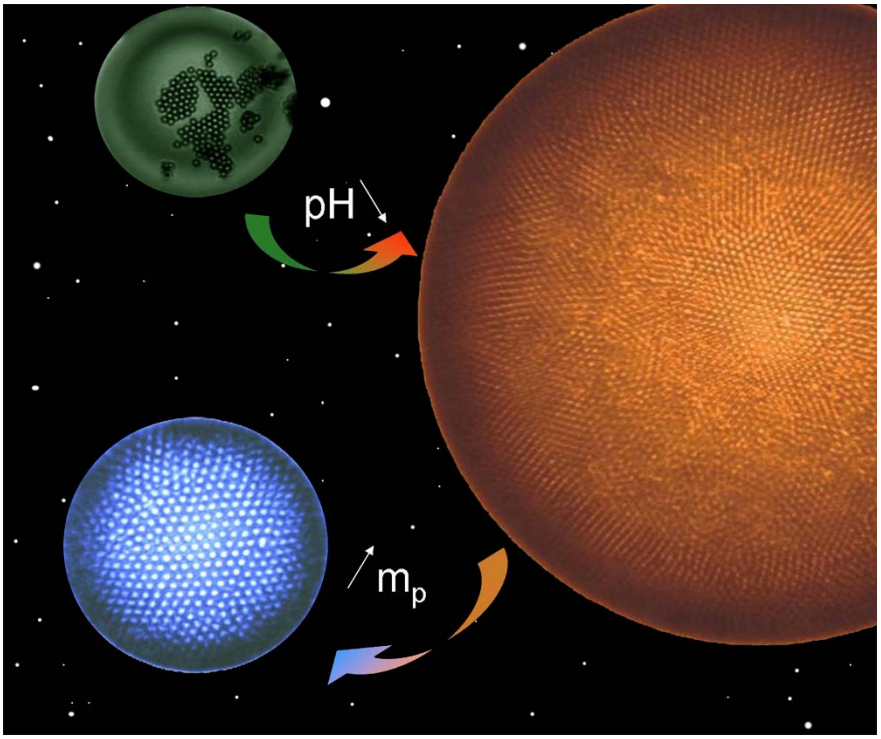

Papers in this issue include:

On the kinetics of nanoparticle self-assembly at liquid/liquid interfaces†

S. Kutuzov,[a] J. He,[b] R. Tangirala,[b] T. Emrick,[b] T. P. Russell[b] and A. Böker*[ac]

Received 2nd July 2007, Accepted 1st November 2007
First published as an Advance Article on the web 13th November 2007
DOI: 10.1039/b710060b

We investigate the concentration and size dependent self-assembly of cadmium selenide nanoparticles at an oil/water interface. Using a pendant drop tensiometer, we monitor the assembly kinetics and evaluate the effective diffusion coefficients following changes in the interfacial tension for the early and late stages of nanoparticle adsorption. Comparison with the coefficients for free diffusion reveals the energy barrier for particle segregation to the interface. The formation of a nanoparticle monolayer at the oil/water interface is characterised by transmission electron microscopy.

Introduction

The hierarchical organization of inorganic and organic nanoparticles, nanocrystals and other nanometer-sized objects constitutes an important field of research aiming to devise new materials for encapsulation and delivery, sensing, data storage, *etc*. Size variation of nanoparticles strongly affects their physical properties (optical, electrical, magnetic, *etc*.). Therefore, size dependent assembly of these particles is an important prerequisite for the construction of novel materials or devices, *i.e*. hierarchical, three-dimensional assemblies. Thus, strategies to organize nanoparticles in a controlled manner in three dimensions need to be devised. A simple and generally used technique is the organization through self-assembly processes at liquid or solid interfaces.[1–9]

Three different approaches to control ordering of nanoparticles *via* self-assembly processes have been used:

(1) Three-dimensional ordering by crystallization of the nanoparticles to produce so-called "colloidal crystals".[10–12]

(2) Wet-deposition using directed supramolecular interactions between a template and the nanoparticles.[13,14]

(3) Assembly of the particles at liquid/liquid interfaces driven by a decrease of the interfacial tension.[15]

Each of the above-described approaches obtains different levels of order: a sedimentation and precipitation process yields a high degree of ordering. Due to the low rate of sedimentation, several weeks may be required to generate a highly ordered structure. The second strategy leads to the formation of irregular arrays due to the initial strong attachment of the particles to the substrate.[16] Annihilation of defects after assembly is not possible. The segregation of the particles to the liquid/liquid interface, on the other hand, affords sufficient mobility to nanoparticles at the interface, which results in the formation of highly ordered nanoparticle arrays[17,18] provided the components equilibrate between aggregated and non-aggregated states, or adjust their positions relative to one another once in an aggregate. Thus, fluid interfaces are ideal templates for such a process. In addition, the fluid/fluid interface provides easy access to the nanoparticles for possible particle replacement at the interface,[3] their chemical modification *via* reactions of attached ligands with reagents in either or both fluids, or cross-linking to form an ultrathin network.[2,19]

Recently, nanometer-sized CdSe particles were found to stabilize water/oil emulsions in a manner similar to that seen with Pickering emulsions of micron-sized colloids. The nanoparticle assembly was demonstrated using fluorescence confocal microscopy and it was shown that densely packed assemblies of ligand-covered nanoparticles could be cross-linked *via* free radical or ring opening metathesis polymerisation (ROMP) methods to yield stable, mechanically-robust capsules and ultrathin membranes.[2,20]

Here the kinetics of nanoparticle adsorption at the fluid interface as a function of the size and bulk concentration of the nanoparticles is discussed. The change in interfacial tension was studied using a pendant drop tensiometer. In addition, TEM was used to examine the evolution in the packing of the nanoparticles during the course of the adsorption process.

Experimental

Synthesis

TOPO-stabilized CdSe nanoparticles were synthesized using standard techniques as described in the literature.[21] The nanoparticles were grown to the requisite size and repeatedly precipitated in methanol to remove excess ligand. UV-Vis and thermogravimetric analysis (TGA) measurements confirmed complete removal of the free TOPO ligands.

Electron microscopy

Transmission electron microscopy (TEM) was performed using 200 mesh Cu grids coated with a ~30 nm thick carbon membrane, on a Zeiss CEM902 microscope operated at 80 kV.

[a] *Lehrstuhl für Physikalische Chemie II, Universität Bayreuth, D-95440 Bayreuth, Germany*
[b] *Department of Polymer Science & Engineering, University of Massachusetts, Amherst, MA 01003, USA*
[c] *Bayreuther Zentrum für Kolloide und Grenzflächen (BZKG), D-95440 Bayreuth, Germany. E-mail: alexander.boeker@uni-bayreuth.de*

† Electronic supplementary information (ESI) available: Sketch of pendant drop apparatus. See DOI: 10.1039/b710060b

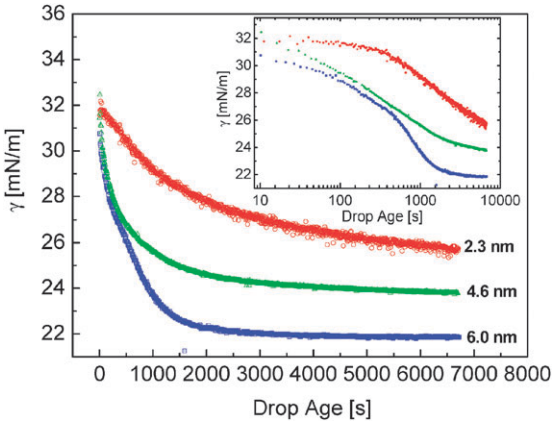

Fig. 1 Time dependence of the interfacial tension for the adsorption of CdSe–TOPO nanoparticles of different diameters at the same bulk molar concentrations ($(3.75 \pm 0.6) \times 10^{-6}$ mol L^{-1}) at the toluene/water interface.

Tensiometer measurements

The dynamic surface tension of the CdSe nanoparticles at the toluene/water interface was measured using the pendant drop method (OCA20, Dataphysics, Stuttgart). The setup of the pendant drop apparatus is shown schematically in the ESI (Fig. 1).† This method has proven to be a useful tool for the investigation of the time dependent evolution of the interfacial tension of classical surfactants, proteins or semiconductor nanoparticles from dilute and semi-dilute solutions.[22–24] Computer automation allowed rapid acquisition of the drop image, edge detection, and fitting of the Laplace–Young equation to determine the interfacial tension. We performed the measurements with a water drop (Milli-Q Academic A-10 system, Millipore, Eschborn, saturated with toluene) immersed in a toluene solution of the nanoparticles. All experiments were performed at room temperature (22 ± 1 °C).

To image the structure formed by the particle assemblies at the toluene/water interface as a function of time, a small drop of water was placed on a TEM grid and then immersed in a nanoparticle solution, allowing the nanoparticle adsorption to proceed for a desired period of time that paralleled the tensiometer measurements. Subsequently the grid was removed from the solution and the water was extracted with dust free paper from below. The grid was then slowly dried in air.

Results and discussion

Size dependence of the interfacial assembly

In Fig. 1 a series of pendant drop tensiometer measurements for particles of 2.3, 4.6 and 6.0 nm diameter at the same molar concentration $(3.75 \pm 0.6) \times 10^{-6}$ mol L^{-1} is shown. The interfacial tension decreases with time and, finally, approaches an equilibrium value, that decreases with increasing particle size. With 6 nm particles the interfacial tension decreases from 33 to $\sim$21.8 mN m^{-1}, while with 4.6 nm particles it decreases to $\sim$23.8 mN m^{-1}, and with the smallest 2.3 nm particles a value of 25.7 mN m^{-1} is observed after $\sim$2 h. In the inset in Fig. 1, these data are plotted on a logarithmic time scale which points to different stages of adsorption characterized by different slopes. At the early stages of adsorption ($t \rightarrow 0$), the interfacial tension rapidly decreases. Subsequently, the decrease in interfacial tension slows, and, finally, the change in interfacial tension decreases further and the nanoparticle assembly attains a dynamic equilibrium where the adsorption and desorption of the nanoparticles proceed with the same rate. Under these conditions the maximum coverage of the interface with nanoparticles is reached ($t \rightarrow \infty$). In this respect, Fig. 1 shows that only the largest particles have reached a constant interfacial tension, and with decreasing nanoparticle size the rate of adsorption of the nanoparticles decreases.

This observation can be explained as follows: the assembly of the nanoparticles at the oil/water (o/w) interface leads to a decrease of the total free energy. The initial high interfacial energy, E_0, between oil (O) und water (W) can be reduced to E_1, a change of ΔE_1 by the placement of the one nanoparticle with an effective radius r[25,26] at the interface. ΔE_1 is given by

$$E_0 - E_1 = \Delta E_1 = -\frac{\pi \cdot r^2}{\gamma_{O/W}} \cdot [\gamma_{O/W} - (\gamma_{P/W} - \gamma_{P/O})]^2, \quad (1)$$

where the three contributions to the interfacial energy arise from the particle/oil ($\gamma_{P/O}$), the particle/water ($\gamma_{P/W}$), and the oil/water interfaces ($\gamma_{O/W}$). From eqn (1) it is evident that for a given system with fixed $\gamma_{P/O}$, $\gamma_{P/W}$, $\gamma_{O/W}$ and at the same temperature influence in terms of k_BT the stability of the particle assembly increases with increasing r. For microscopic particles, the decrease in the energy per particle is much larger than the thermal energy, k_BT, so the particles are strongly held to the interface. However, with nanoparticles the energy gain by adsorbing a particle at the interface is small, of order of k_BT. For example, based on the reported values for the toluene/water system:[3] $\gamma_{O/W}$ $\sim$35.7 mN m^{-1}, $\gamma_{P/O}$ $\sim$15 mN m^{-1} and $\gamma_{P/W}$ $\sim$40 mN m^{-1}, we calculate ΔE_1 to be ~ -3.3 k_BT, -4.9 k_BT and -13.1 k_BT for the 2.3, 4.6 and 6.0 nm diameter nanoparticles, respectively. Consequently, the nanoparticles can be easily displaced from the interface, leading to a continuous particle exchange at the interface. This exchange occurs more rapidly and more readily with decreasing size of the nanoparticle and at the same particle concentration, the coverage of the interface will be more complete with larger particles.

To gain further insight into the structures formed at the interface, we investigated the behavior of 6 nm particles at the toluene/water interface by pendant drop tensiometry and simultaneously collected TEM samples. Fig. 2 shows a representative example of the evolution of the surface tension with time for 6.0 nm CdSe nanoparticles at a particle concentration of 1.58×10^{-6} mol L^{-1} in the bulk solution. Fig. 3 shows a series of TEM images of the particle assemblies at the interface taken at the adsorption times indicated in Fig. 2 (the numbering in Fig. 2 corresponds to the numbers of the TEM images). From the tensiometer data and the TEM images one can infer that the interfacial energy rapidly decreases with increasing number of particles assembling at the interface. The logarithmic plot in the inset of Fig. 2 reveals the

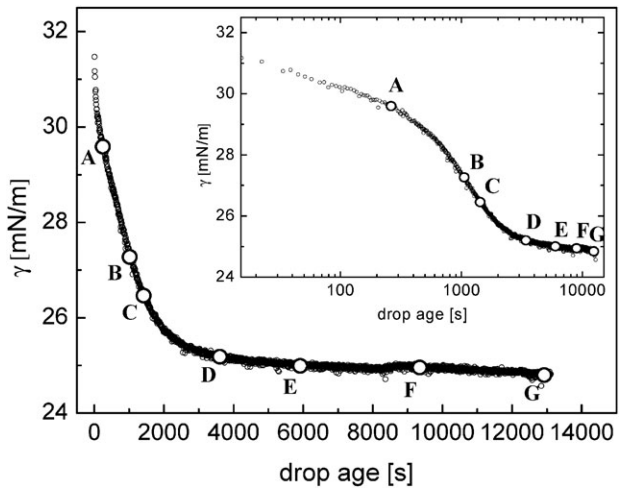

Fig. 2 Time dependence of the interfacial tension of the toluene/water interface in the presence of 6.0 nm CdSe nanoparticles (c = 1.58×10^{-6} mol L^{-1}). The circles mark the time at which the TEM samples were prepared.

previously described regimes with different slopes. In combination with Fig. 3, we can quantitatively distinguish between different adsorption stages. The early stage of the adsorption is dominated by the diffusion of the particles to the free toluene/water interface. The number of particles at the interface increases rapidly, leading to a coverage of ~20% after 230 s (calculated from the large area analogues of the TEM images in Fig. 3). After 1400 s, the coverage has risen to 40%. The decrease in interfacial tension slows down dramatically after ~3500 s (coverage more than 50%), leading to the final stage of adsorption ($t \rightarrow \infty$). Here, we anticipate that the adsorption of new particles is increasingly hindered by the desorption of particles from the interface and rearrangement of particles already adsorbed at the interface. Once the rate of adsorption and desorption are equal, a dynamic equilibrium is achieved and a maximum coverage of the interface with nanoparticles is reached (Fig. 3 E: 80%, F: 90%).

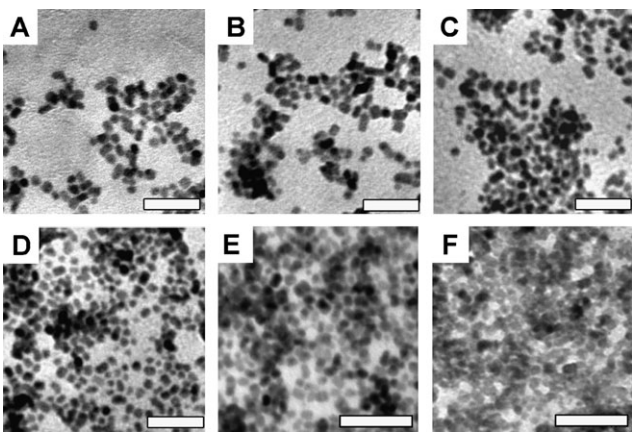

Fig. 3 Series of TEM images of 6 nm nanoparticle adsorption to the toluene/water interface at different adsorption times as marked in Fig. 2: (A) 230, (B) 1060, (C) 1400, (D) 3514, (E) 4700 and (F) 10 800 s. Structure formation *via* nucleation and growth of clusters can be seen. Scale bar: 40 nm.

In addition to the coverage, the TEM series also yields insight into the mechanism of structure formation. Initially nanoparticles organize into the clusters, the size and form of which changes with time. This suggests that there is a weak favorable interaction between the nanoparticles. Based on published data,[27,28] this is, more than likely, dipole–dipole interactions. With time the clusters grow and finally form large islands (Fig. 3D–F), leading to almost complete coverage of the oil/water interface.

Concentration dependence of the interfacial assembly

Fig. 5A and 6A illustrate the experimentally obtained $\gamma(t)$-curves for 2.3 and 6 nm diameter CdSe nanoparticles at different particle concentrations in toluene. With changing concentration, the surface tension at which the system attains dynamic quasi-equilibrium at $t \rightarrow \infty$ changes.[24,29] Here, "quasi-equilibrium" means, that the system reaches an almost full interfacial coverage in form of a particle monolayer. As shown before, from the logarithmic plots in Fig. 5B and 6B the particle assembly at the interface undergoes different stages: (i) free diffusion to the interface, (ii) continuing adsorption of nanoparticles, including ordering and rearrangement of the nanoparticles at the interface and (iii) additional packing leading to the formation of a monolayer at the interface. As discussed earlier, it takes the smaller nanoparticles a longer time to reach an equilibrium interfacial tension. From the concentration series, for a fixed size, decreasing the nanoparticle concentration extends the time at which the system reaches equilibrium. So, for 6 nm particles, all concentrations investigated reached a plateau value in the final stage, whereas for the 2.3 nm particles only the highest concentrations come close to such a state. Obviously, the 2.3 nm system does not reach full coverage of the interface. Here we note, that Zeta potential measurements showed that the nanoparticles did not carry any charge. Therefore, we can exclude electrostatic repulsions. From a geometric point of view, one may anticipate that the small particles may pack more closely at the interface and, therefore, cover a larger interfacial area than the 6 nm particles. However, considering the energetic gain in keeping the nanoparticles at the interface (eqn (1)), one has to conclude that the smaller particles also undergo desorption from the interface more often than the larger particles. This may lead to the observed differences in adsorption behavior. For the 6 nm particles, we have shown the interfacial coverage with TEM. For the 2.3 nm particles, we used the Langmuir–Szyszkowski approach to estimate the interfacial coverage. The values of the quasi-static equilibrium surface tension for the CdSe nanoparticle assembly at the water/toluene interface are extracted from the long-time asymptotes in Fig. 4A, and are plotted *versus* the bulk particle concentration in Fig. 6. These interfacial tension values were determined for each concentration at an adsorption time of ~7200 s. The equilibrium interfacial tension decreases with increasing CdSe nanoparticle concentration until a "critical" concentration (c^* = 8.56×10^{-6} mol L^{-1}) is reached, where the interface is saturated (in analogy to typical surfactant).[30] Therefore, at the critical concentration c^*, the density of the adsorbed particles, *i.e.* the coverage, reaches its maximum value

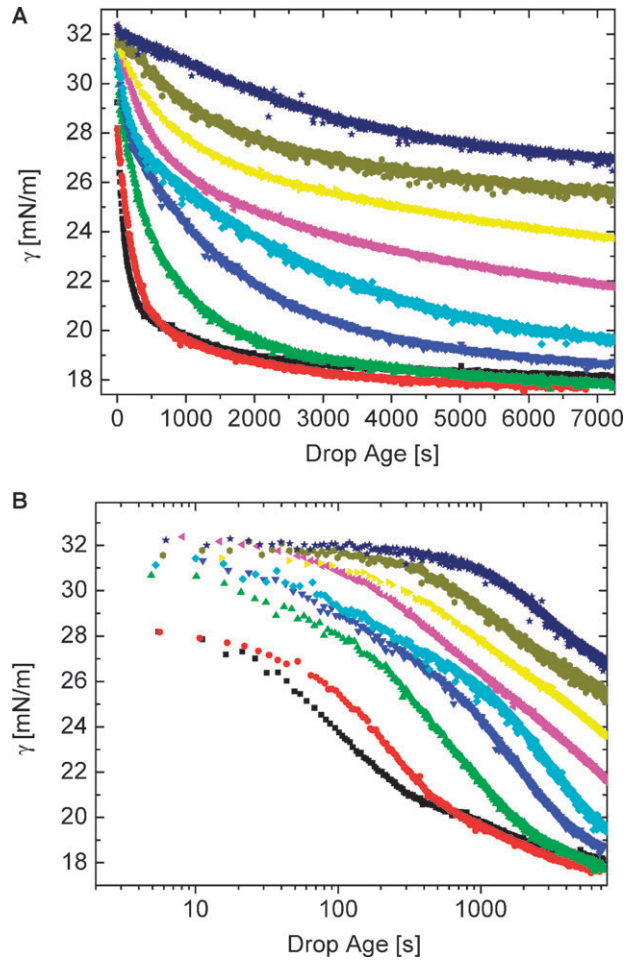

Fig. 4 (A) Time dependence of the interfacial tension at toluene/water interface with 2.3 nm CdSe–TOPO at the different particle concentrations (■ 4.49×10^{-4} mol L^{-1}, ● 2.24×10^{-4} mol L^{-1}, ▲ 1.12×10^{-4} mol L^{-1}, ▼ 5.61×10^{-5} mol L^{-1}, ◆ 2.81×10^{-5} mol L^{-1}, ◀ 1.41×10^{-5} mol L^{-1}, ▶ 7.05×10^{-6} mol L^{-1}, ⬢ 3.50×10^{-6} mol L^{-1}, ★ 1.75×10^{-6} mol L^{-1}). (B) Logarithmic representation of the data in (A).

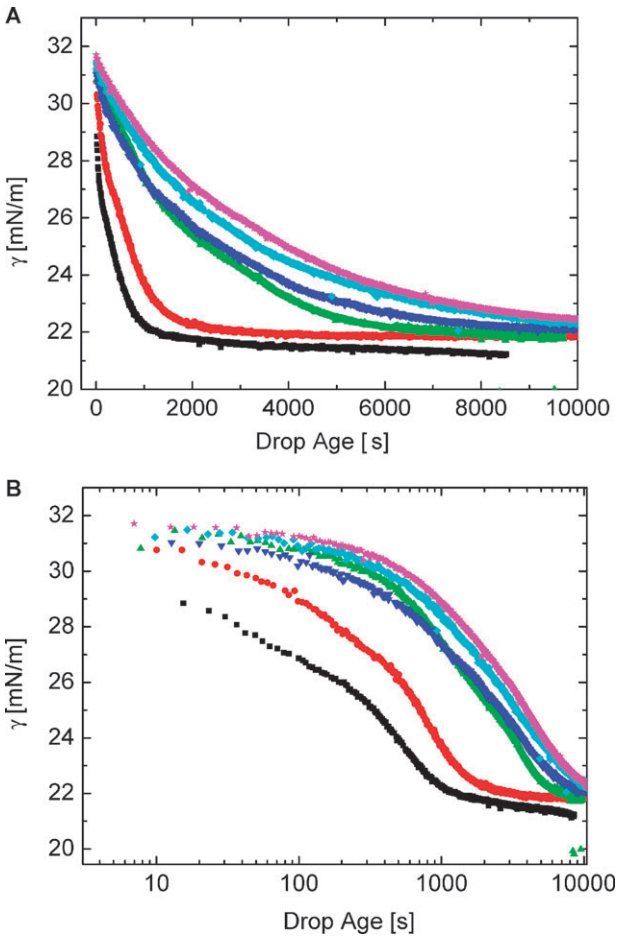

Fig. 5 (A) Time dependence of the interfacial tension at toluene/water interface with 6.0 nm CdSe–TOPO at the different particle concentrations (■ 6.32×10^{-6} mol L^{-1}, ● 3.16×10^{-6} mol L^{-1}, ▲ 1.58×10^{-6} mol L^{-1}, ▼ 7.90×10^{-7} mol L^{-1}, ◆ 3.95×10^{-7} mol L^{-1}, ★ 1.90×10^{-7} mol L^{-1}). (B) Logarithmic representation of the data in (A).

Γ_∞, and remains constant with increasing number of nanoparticles in the bulk, $c_{eq} > c^*$.

To describe an adsorption coupled with bulk diffusion of the interface-active nanoparticles the Langmuir model has been used. The Langmuir model, or localized ideal model, considers the molecules without any interactions adsorbed on localized sites on the interfacial layer and is a good approximation for the equilibrium relationship between the adsorption density Γ at the interface and the particle concentration in the volume phase c.[31] Thus,

$$\Gamma = \Gamma_\infty \cdot \frac{c_{eq}}{a_L + c_{eq}} \qquad (2)$$

Here, c_{eq} is the bulk concentration at quasi-static equilibrium interfacial tension, a_L is the Langmuir parameter (bulk concentration at half surface coverage) and Γ_∞ is the monolayer capacity expressing the maximum amount of nanoparticles that can be accommodated at the interface. At low nanoparticle concentrations, the behavior at the liquid/liquid and air/liquid interfaces is similar to that for surfactant molecules. Hence, at low nanoparticle concentrations, the CdSe solution,

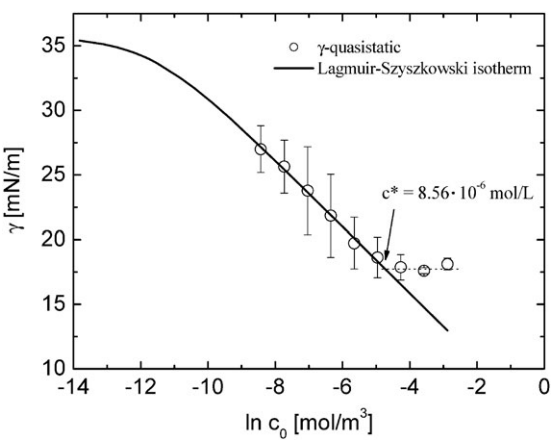

Fig. 6 Quasi-static interfacial tension γ as a function of the logarithmic concentration of 2.3 nm CdSe nanoparticles. The line represents a fit based on the Langmuir–Szyszkowski equation (eqn (4)).

can be considered as ideal. The Gibbs adsorption equation[32]

$$\Gamma = -\frac{1}{R \cdot T}\frac{d\gamma}{d \ln c_{eq}} \qquad (3)$$

and the equilibrium isotherm (2) allow the calculation of the surface tension explicitly as a function of a particle concentration in the volume phase c_{eq}. The combination of eqn (2) and (3) leads to the Langmuir–Szyszkowski isotherm equation[30]

$$\gamma = \gamma_0 - R \cdot T \cdot \Gamma_\infty \cdot \ln\left(1 + \frac{c_{eq}}{a_L}\right), \qquad (4)$$

where γ_0 is the interfacial tension of the pure components. According to Ross and Morrison,[33] the Langmuir–Szyszkowski isotherm can be used to describe the decrease in surface tension of a solution as a function of concentration. It should be noted that the energies of adsorption and desorption of the particles at the interface depend on the surface coverage. With increasing surface coverage, more work is required to insert additional particles onto the interface, and, therefore, the adsorption rate decreases relative to that of desorption. The Szyszkowski model neglects this fact and achieves the best fit of the equilibrium data at low particle concentrations. For a given water/toluene interface $\gamma_{O/W}$ = 35.7 mN m^{-1} and at a constant temperature T = 295.15 K the Langmuir–Szyszkowski isotherm is characterized by a maximum adsorption density, Γ_∞ (2.3 nm) = 1.05×10^{-10} mol cm^{-2}, and the Langmuir parameter, a_L = 8.2×10^{-9} mol cm^{-3} (Fig. 6). The theoretically estimated value for the maximum monolayer capacity is Γ^* (2.3 nm) = 3.61×10^{-11} mol cm^{-2} (shell size of CdSe–TOPO not taken into account) and Γ^* (2.3 nm) = 1.26×10^{-11} mol cm^{-2} (with the CdSe–TOPO shell). Both values are in good agreement with the experimental value Γ_∞. Therefore, these results point to the fact that at higher concentrations even the 2.3 nm particles may reach a full monolayer coverage at the interface.

The Langmuir–Szyszkowski isotherm for the 6 nm particles is characterized by a maximum of the adsorption density Γ_∞ (6.0 nm) = 2.34×10^{-11} mol cm^{-2}. The theoretically-estimated value corresponding to the maximal saturation of an interface by particles is five times less and is equal to Γ^* (6.0 nm) = 3.32×10^{-12} mol cm^{-2}. As expected, the Γ_∞ (6.0 nm) value is also smaller than that of the 2.3 nm nanoparticles, Γ_∞ (2.3 nm). As the plane capacity of the interface is proportional to the square of the particle radius, the increase of the radius of the particles of a factor of 2.6 explains the decrease of the interfacial coverage of about one order of magnitude.

Diffusion to the interface and potential barrier of adsorption

At the early stage of adsorption, a diffusion controlled adsorption kinetics of the CdSe nanoparticles is expected. This process can be quantitatively described by the theory of Ward and Tordai[34] in the following form:[29]

$$\Gamma(t) = 2\sqrt{\frac{D}{\pi}}\left(c_{eq}\sqrt{t} - \int_0^{\sqrt{t}} c(0, t-\tau)d\sqrt{t}\right) \qquad (5)$$

where D is the diffusion coefficient. The time dependence of the dynamic interfacial tension is described by the following asymptotic relations (intermediate application of the Gibbs' adsorption isotherm):[29]

$$\gamma(t) \cong \begin{cases} \gamma_0 - 2 \cdot R \cdot T \cdot c_{eq}\sqrt{\dfrac{Dt}{\pi}}, \quad \text{or} \quad \left.\dfrac{d\gamma}{dt^{1/2}}\right|_{t\to 0} = -2 \cdot R \cdot T \cdot c_{eq}\sqrt{\dfrac{D}{\pi}} & (t \to 0), \\ \gamma_\infty + \dfrac{R \cdot T \cdot \Gamma_\infty^{\,2}}{c_{eq}}\sqrt{\dfrac{\pi}{4 \cdot D' \cdot t}}, \quad \text{or} \quad \left.\dfrac{d\gamma}{dt^{-1/2}}\right|_{t\to\infty} = \dfrac{R \cdot T \cdot \Gamma^2_\infty}{c_{eq}}\sqrt{\dfrac{\pi}{4 \cdot D'}} & (t \to \infty) \end{cases} \qquad (6)$$

where γ_∞ is the interfacial tension at maximum adsorption.

Based on these approximations, the diffusion coefficients D (for $t \to 0$) and D' (for $t \to \infty$) at different nanoparticle concentrations were calculated for the 2.3 nm particles and the results were plotted in Fig. 7. At small particle concentrations ($\sim c_{2.3\ nm} = 1.75 \times 10^{-6}$ mol L^{-1}), the diffusion coefficient is similar to the value predicted by Stokes' theory: D_{Stokes} (2.3 nm) = (4.0 ± 1.5) × 10^{-11} m^2 s^{-1}. With increasing particle concentration ($c_{2.3\ nm} = 2.24 \times 10^{-4}$ mol L^{-1}), the diffusion coefficient for long times decreases by three orders of magnitude. Here, we note that the 6.0 nm diameter nanoparticles show a qualitatively similar behavior: at $c_{6\ nm} = 1.9 \times 10^{-7}$ mol L^{-1} the diffusion coefficient is in the Stokes' region: D_{Stokes} (6 nm) = (4.6 ± 0.6) × 10^{-11} m^2 s^{-1}. Increasing the particle concentration ($c_{6\ nm} = 6.3 \times 10^{-6}$ mol L^{-1}), also decreases the diffusion coefficient at long times by three orders

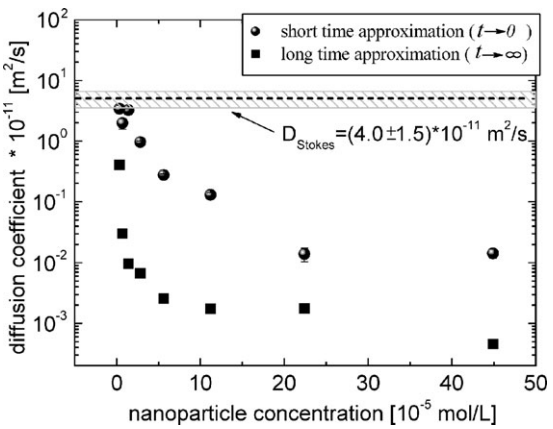

Fig. 7 Calculated diffusion coefficients of the 2.3 nm sized CdSe nanoparticles at room temperature at different particle concentrations for $t \to 0$ and $t \to \infty$ (eqn (6)).

of magnitude. For all particle sizes at each concentration, we find the diffusion coefficients for the short time limit to be larger than for the long time limit. The diffusion coefficients D and D' decrease when the particle concentration is increased. At a low concentration D and D' reach the diffusion limit as predicted by Stokes–Einstein equation. These observations point to the fact that with increasing nanoparticle adsorption at the interface the adsorption switches from a diffusion controlled to an interaction controlled process, *i.e.* at higher concentrations or longer adsorption times, the reduction of the diffusion coefficient can be attributed to the interaction between the particles close to the oil/water-interface. This interaction is a result of the collisions of the nanoparticles approaching the interface from the bulk with nanoparticles that are already adsorbed to the interface or that desorb from it due to thermal fluctuations. Thus, one nanoparticle can adsorb to the oil/water-interface only if free space is available. During the course of the adsorption, with increasing particle concentration in the sub-layer (which is defined as the region of the bulk solution, immediately next to the interface with a thickness of the few particle diameters[34,35]), the number of collisions increases. In addition, the desorbing nanoparticles hinder the adsorption of each additional nanoparticle from the bulk to the interface. This suggests the existence of an effective potential barrier close to the interface, which manifests itself by restraining the particle movement normal to the interface in the range of the sub-layer. Consequently, the motion of the particles around the interface involves two mechanistic steps: (i) the diffusion-controlled particle motion from the solution volume to the sub-layer and (ii) overcoming the potential barrier ΔE_p between the real interface and the bulk. The position of the barrier and its width depends on the strength of the inter-particle interactions close to the interface. It should be mentioned that at very low nanoparticle concentrations the sub-layer vanishes as it becomes too broad and indistinguishable from the bulk. This notion is supported by the fact that, at low particle concentrations, the diffusion coefficients approach the Stokes' diffusion coefficient, which is a direct consequence of the rare interaction between the nanoparticles and the resulting free diffusion to the oil/water-interface. From our observations, we have developed a model of the particle adsorption at the liquid/liquid interface, schematically presented in Fig. 8, which combines Pieranski's interface energy well for the already adsorbed nanoparticles (red line) with the predicted energy barrier for the incoming particles from the bulk phase (green line).

In view of the proposed adsorption model: initially (early stage of adsorption in the Fig. 5B and 6B) the interface is essentially empty and every particle colliding with the interface can adsorb freely. Thus, the sub-layer concentration rapidly approaches zero. Therefore, at the early stage of the process, there is no energy barrier between the interface and the sub-interface. The concentration gradient produced by this adsorption causes the diffusion-controlled movement of the nanoparticles from the bulk into the sub-layer until its concentration is equal to the bulk. To allow for a concentration balance, the bulk is considered an infinite reservoir of nanoparticles. The further course of the particle adsorption is characterized by the presence of the adsorbed nanoparticles

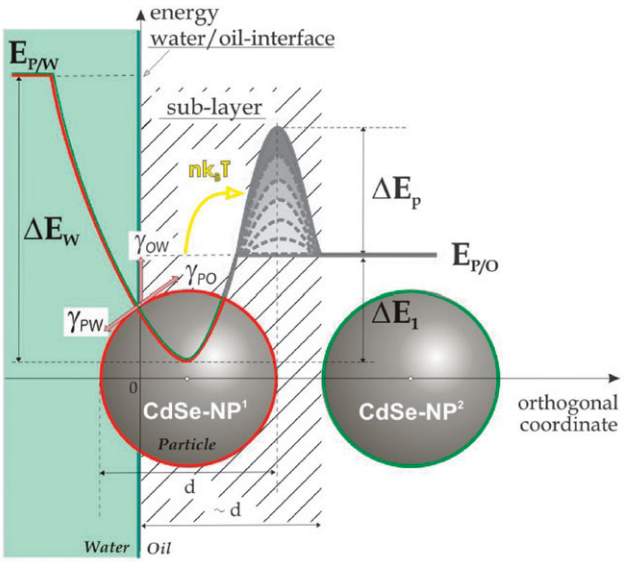

Fig. 8 Schematic energetic diagram of spherical CdSe nanoparticles at the oil/water interface (CdSe–NP^1) and in the bulk (CdSe–NP^2). With γ: interfacial tension, P: particle, W: water, O: oil, d: effective nanoparticle diameter. The hatched region presents the area of the sub-layer. The red line presents the estimated form of the interfacial energy well of the depth ΔE_1 for the already adsorbed nanoparticle CdSe–NP^1 (according to ref. 25). Green lines represent the form and position of the potential barrier for any incoming CdSe–NP^2 from the bulk. The increase of the ΔE_p is marked with a color gradient. The yellow arrow shows the direction of an escape of a thermally activated nanoparticle from the interface.

at the interface (a complete interfacial coverage has not yet been reached), *i.e.* there is a decreasing area where the incoming particles can adsorb. With increasing interface coverage, the incoming particles are repelled by the adsorbed solute, and as a result, they remain outside the sub-layer. Thus, the adsorption is less diffusion-controlled. Consequently, a potential barrier emerges that increases with increasing interfacial coverage. The analysis of the estimated values of diffusion coefficients confirms the notion of a non-diffusional adsorption for later stages. For a certain particle concentration, the diffusion of the CdSe–TOPO nanoparticles is hindered with increasing adsorption time, *i.e.* the diffusion coefficient derived from the early stage fit ($t \rightarrow 0$) is larger than for the later stage ($t \rightarrow \infty$), because the limiting step is the reaction, *i.e.* particle exchange and displacement at the interface. In addition, for both approximations, we observe that the diffusion coefficient also decreases with increasing initial concentration of the nanoparticles in the bulk (Fig. 7) which also points to an increasingly reaction-limited process. Finally, the coverage of the oil/water-interface with the nanoparticles is almost complete. Adsorption of the new particles from the bulk is possible only if there is a permanent thermal particle release and exchange from the interface into bulk, increasing the particle concentration in the sub-layer. As soon as the number of the particles close to the interface increases, the osmotic pressure increases as well. Now, before the incoming particle finds an unoccupied place at the interface, it collides with a large number of neighbors, and therefore the particle concentration

in the sub-layer region increases temporarily, which finally leads to a retardation of the overall diffusion process and the build-up of a potential barrier.

Based on the assumption that the TOPO-covered nanoparticles act as elastic balls, we assume a symmetric form for the potential barrier (Fig. 8). The activation energy ΔE_p, *i.e.* the potential barrier for adsorption in the case of the reaction controlled adsorption, can be calculated from the effective diffusion coefficient D_{eff} by:[36,37]

$$D_{eff} = D^* \exp\left(-\frac{\Delta E_p}{k_B T}\right), \qquad (7)$$

For the free diffusion case without energy barrier, D^* should be equal to the diffusion coefficient predicted by Stokes–Einstein. Indeed, Fig. 7 demonstrates that the values calculated for low particle concentrations, as well as the early stages of adsorption (short time approximation), approach the expected Stokes diffusion coefficient D_{Stokes}. As D_{eff} we used the values obtained from long-time approximation (see eqn (6)). The values of ΔE_p calculated by the eqn (7) yield a magnitude of the energy barrier, ΔE_p, of about 10^{-20} J for all the nanoparticles, regardless of size, investigated in this study. We note that this is a few $k_B T$, and coincides with the desorption energy calculated for 2.3 and 6 nm particles, according to eqn (1). This result confirms the idea, that at the higher nanoparticle concentrations the probability of the one single nanoparticle diffusing to the interface is determined by the desorption rate of the already adsorbed nanoparticles. In this situation the energy of the thermally activated desorption $k_B T$ can be considered as the measure of the activation energy ΔE_p.

It should be mentioned that, in general, the diffusion of the nanoparticles along the interface can lead to generation of the "free" places at the interface by particle rearrangement and close packing, and thus, can further influence the process of adsorption. In fact, in-plane diffusion of the nanoparticles at a fully covered interface was found to be about four orders of magnitude slower than that of the particles in solution ($D_{interface} \sim 10^{-14}$ m^2 s^{-1}).[38] Therefore, at the late stage of adsorption the most probable mechanism to create a free space at the oil/water interface is by desorption of a particle rather than lateral diffusion and reordering of the nanoparticle interfacial assembly.

Conclusions

In this study, we have demonstrated that the pendant drop technique can be used to characterize the adsorption behavior of the TOPO-covered CdSe nanoparticles at the oil/water interface. From the time evolution of the interfacial tension, we could infer the characteristics of early ($t \rightarrow 0$) and late stages ($t \rightarrow \infty$) of the adsorption process, *i.e.* free diffusion to the interface, followed by continuing adsorption of particles including ordering and rearrangement of the nanoparticles at the interface and finally additional packing leading to formation of a monolayer at the interface. TEM images of the oil/water interface taken during the nanoparticle adsorption process revealed a nucleation and growth mechanism for the monolayer formation. Moreover, it was shown that the self-assembly process changes from diffusion-controlled to interaction-controlled with increasing interfacial coverage. In addition, the respective potential barrier for nanoparticle adsorption to the interface was calculated from the diffusion constants of the late stage of adsorption and found to be on the order of the desorption energy for a single particle from the interface. This fact supports the notion of an interaction-controlled adsorption at the late stage of the process.

Acknowledgements

The authors would like to thank Larisa Tsarkova and Larysa Samokhina for helpful discussions. We also acknowledge Martha Azuero and Thomas Czubak for help with the preparation of the TEM samples and the tensiometer measurements. This work was carried out in the framework of the Sonderforschungsbereich 481 (TP B10) funded by the Deutsche Forschungsgemeinschaft (DFG). Moreover, this work was supported by the US Department of Energy, Office of Basic Energy Science, the Army Research laboratory through the MURI program, and the NSF supported MRSEC at the University of Massachusetts Amherst.

References

1 A. Böker, J. He, T. Emrick and T. P. Russell, *Soft Matter*, 2007, **3**, 1231–1248.
2 Y. Lin, H. Skaff, A. Böker, A. D. Dinsmore, T. Emrick and T. P. Russell, *J. Am. Chem. Soc.*, 2003, **125**, 12690–12691.
3 Y. Lin, H. Skaff, T. Emrick, A. D. Dinsmore and T. P. Russell, *Science*, 2003, **299**, 226–229.
4 A. D. Dinsmore, M. F. Hsu, M. G. Nikolaides, M. Marquez, A. R. Bausch and D. A. Weitz, *Science*, 2002, **298**, 1006–1009.
5 A. Böker, Y. Lin, K. Chiapperini, R. Horowitz, M. Thompson, V. Carreon, T. Xu, C. Abetz, H. Skaff, A. D. Dinsmore, T. Emrick and T. P. Russell, *Nat. Mater.*, 2004, **3**, 302–306.
6 D. Y. Wang and H. Möhwald, *J. Mater. Chem.*, 2004, **14**, 459–468.
7 Y. Lin, A. Böker, J. He, K. Sill, H. Xiang, C. Abetz, X. Li, J. Wang, T. Emrick, S. Long, Q. Wang, A. Balazs and T. P. Russell, *Nature*, 2005, **434**, 55–59.
8 *Colloidal Particles at Liquid Interfaces*, ed. B. P. Binks and T. S. Horozov, Cambridge University Press, Cambridge, 2006.
9 J. He, R. Tangirala, T. Emrick, T. P. Russell, A. Böker, X. Li and J. Wang, *Adv. Mater.*, 2007, **19**, 381–385.
10 A. D. Dinsmore, J. C. Crocker and A. G. Yodh, *Curr. Opin. Colloid Interface Sci.*, 1998, **3**, 5–11.
11 C. B. Murray, C. R. Kagan and M. G. Bawendi, *Science*, 1995, **270**, 1335–1338.
12 P. Jiang, J. F. Bertone and V. L. Colvin, *Science*, 2001, **291**, 453–457.
13 N. Lu, X. D. Chen, D. Molenda, A. Naber, H. Fuchs, D. V. Talapin, H. Weller, J. Muller, J. M. Lupton, J. Feldmann, A. L. Rogach and L. F. Chi, *Nano Lett.*, 2004, **4**, 885–888.
14 K. Nagayama, *Colloids Surf., A*, 1996, **109**, 363–374.
15 B. P. Binks, *Curr. Opin. Colloid Interface Sci.*, 2002, **7**, 21–41.
16 J. Tang, H. Birkedal, E. W. McFarland and G. D. Stucky, *Chem. Commun.*, 2003, 2278–2279.
17 G. M. Whitesides and B. Grzybowski, *Science*, 2002, **295**, 2418–2421.
18 G. M. Whitesides and M. Boncheva, *Proc. Natl. Acad. Sci. U. S. A.*, 2002, **99**, 4769–4774.
19 Y. Lin, A. Böker, J. He, J. T. Russell, P. Carl, A. Fery, S. Long, Q. Wang, K. Sill, T. Emrick, H. Zettl, D. Cookson, P. Thiyagarajan and T. P. Russell, *Angew. Chem., Int. Ed.*, 2005.
20 H. Skaff, Y. Lin, R. Tangirala, K. Breitenkamp, A. Böker, T. P. Russell and T. Emrick, *Adv. Mater.*, 2005, **17**, 2082–2086.
21 H. Skaff, M. F. Ilker, E. B. Coughlin and T. Emrick, *J. Am. Chem. Soc.*, 2002, **124**, 5729–5733.

22 N. Glaser, D. Adams, A. Böker and G. Krausch, *Langmuir*, 2006, **22**, 5227.
23 A. V. Makievski, R. Wustneck, D. O. Grigoriev, J. Kragel and D. V. Trukhin, *Colloids Surf., A*, 1998, **143**, 461.
24 S.-Y. Lin, K. McKeigue and C. Maldarelli, *AlChE J.*, 1990, **36**, 1785.
25 P. Pieranski, *Phys. Rev. Lett.*, 1980, **45**, 569–572.
26 B. P. Binks and S. O. Lumsdon, *Langmuir*, 2000, **16**, 8622–8631.
27 L.-s. Li and A. P. Alivisatos, *Phys. Rev. Lett.*, 2003, **90**, 0974021–0974024.
28 X. Wang, C.-K. Shih, J. Xu and M. Xao, *Appl. Phys. Lett.*, 2006, **89**, 113114.
29 V. B. Fainerman, A. V. Makievski and R. Miller, *Solids Surf. A*, 1994, **87**, 61–75.
30 U. Teipel and N. Aksel, *Chem. Eng. Technol.*, 2001, **24**, 393–400.
31 R. Miller, *Colloid Polym. Sci.*, 1981, **259**, 375–381.
32 B. P. Binks, *Modern Aspects of Emulsion Science*, The Royal Society of Chemistry, 1998.
33 S. Ross and I. D. Morrison, *J. Colloid Interface Sci.*, 1982, **91**, 244–247.
34 A. F. H. Ward and L. Tordai, *J. Chem. Phys.*, 1946, **14**, 453–461.
35 R. Miller and G. Kretzschmar, *Adv. Colloid Interface Sci.*, 1991, **37**, 97–121.
36 F. Ravera, L. Liggieri and A. Steinchen, *J. Colloid Interface Sci.*, 1993, **156**, 109–116.
37 L. Liggieri, F. Ravera and A. Passerone, *Colloids Surf., A*, 1996, **114**, 351–359.
38 Y. Lin, A. Böker, H. Skaff, D. Cookson, A. D. Dinsmore, T. Emrick and T. P. Russell, *Langmuir*, 2005, **21**, 191–194.

